Electronic structure of a buried two-dimensional antiferromagnetic layer: Experimental and theoretical investigation of Ag/Cr/Ag(001)

Jayanta Das,[1,2] Sananda Biswas,[3,4,5] Kanchan Ulman,[4,5] Rajdeep Banerjee,[5] Gaurav Gautam,[5,6] Asish K. Kundu,[2,4]
Shobhana Narasimhan,[5] and Krishnakumar S. R. Menon[2,*]

[1]*Department of Physics, Maharaja College, Ara, Bihar, 802301, India*
[2]*Surface Physics and Material Science Division, Saha Institute of Nuclear Physics, 1/AF Bidhannagar, Kolkata 700064, India*
[3]*Institut für Theoretische Physik, Goethe-Universität Frankfurt, 60438, Frankfurt am Main, Germany*
[4]*The Abdus Salam International Centre for Theoretical Physics, Strada Costiera 11, Trieste, Italy*
[5]*Theoretical Sciences Unit, Jawaharlal Nehru Centre for Advanced Scientific Research, Jakkur, Bangalore 560064, India*
[6]*Department of Physics, Indian Institute of Technology, Kanpur, 280016, India*

We have investigated the electronic structure of monolayer Cr deposited on Ag(001), using angle-resolved photoemission spectroscopy (ARPES) measurements and density functional theory (DFT) calculations. It is favorable for the Cr layer to be buried one layer deep, resulting in a 1 Ag/1 Cr/Ag(001) sandwich structure with the moments on the Cr atoms aligned antiferromagnetically in a $c(2 \times 2)$ arrangement. Both experiment and theory agree well on the measured/calculated band dispersions and their intensities. Two relatively flat bands arise from antiferromagnetic Cr $3d$ states; in addition, quantum well states with strong curvatures are prominent near both the $\overline{X}$ and $\overline{M}$ points of the surface Brillouin zone. Our results suggest that the buried Cr monolayer in Ag(001) could serve as a prototypical system to study two-dimensional antiferromagnetism in the presence of weak electronic correlation effects.

I. INTRODUCTION

The magnetic properties of ultrathin films often differ dramatically from those of the corresponding bulk systems. This is of particular interest given their importance in technological applications such as magnetic memory storage and spintronics. The magnetic structure is affected by lowering the dimensionality, and can also be further modified by alloying, adsorption, and surface reconstruction [1–11].

Interactions with the underlying substrate can also alter their magnetic moments and spin structure [12–14]. For example, when Fe atoms are arranged in a freestanding monolayer with a triangular lattice, the magnetic moments are found to be ferromagnetically aligned with a moment of $\sim 3\mu_B$. While this remains almost unchanged when the Fe monolayer is deposited on a Pd(111) substrate, the magnetic structure is significantly modified on a Ru(0001) substrate to an antiferromagnetic (AFM) Néel state with Fe moments of $2.75\mu_B$ [9]. Moreover, on both substrates, the Fe moments are significantly enhanced with respect to the bulk value of $2.2\mu_B$ per atom. When it comes to the square lattices of the face-centered-cubic (001) surfaces, calculations have shown that there is a general tendency for overlayers of the late transition metals (Fe, Co, and Ni) to assume ferromagnetic (FM) configurations when placed on substrates such as Cu, Ag, and Pd, whereas the early transition metals (V, Cr, and Mn) favor AFM $c(2 \times 2)$ configurations [15–20].

The lowering of dimensionality has an especially striking impact in the case of Cr with its half-filled $3d$ orbitals. Bulk Cr is a body-centered-cubic (bcc) metal featuring an incommensurate spin-density wave with a magnetic moment of $\sim 0.59\mu_B$ per atom [21,22]. *Ab initio* density functional theory (DFT) calculations have shown [23] that there is a giant enhancement of magnetic moments in the Cr monolayer on Ag(001), with a moment of $4.45\mu_B$ per atom. This enhancement is partly driven by the increase in nearest-neighbor distance from 2.49 Å in the bcc bulk to 2.88 Å in the monolayer, where the spins are arranged in a $c(2 \times 2)$ AFM ordering.

The experimental lattice constants of bulk chromium and silver are $a(\text{Cr}) = 2.88$ Å and $a(\text{Ag}) = 4.09$ Å, respectively. Thus, we have the relation $a(\text{Cr}) \approx a(\text{Ag})/\sqrt{2}$, suggesting that it should be possible to grow Cr epitaxially on Ag(001) with the surface unit cells of the overlayer and substrate rotated by 45° with respect to one another. The lattice mismatch is very small, $\sim 0.3\%$. However, there has been some disagreement in the literature about whether or not it is possible to experimentally obtain flat monolayer growth of Cr on an Ag(001) substrate, as well as regarding the resulting magnetic structure. The group of Gewinner reported that it was indeed possible to grow a monolayer of Cr on Ag(001) [24–29], and claimed, based on exchange-scattered low-energy electron diffraction (LEED) measurements and photoemission studies that the magnetic structure corresponded to a $c(2 \times 2)$ AFM phase [30–32]. However, scanning tunneling microscopy (STM) studies on the same system did not support the existence of flat monolayer growth [33,34]. Previous detailed growth optimization and characterization studies in our group have confirmed that at moderate growth temperatures (around 428 K), Cr on Ag(001) indeed forms a flat monolayer which is ordered in the $c(2 \times 2)$ AFM structure [35,36].

*krishna.menon@saha.ac.in

However, our previous studies have revealed that, despite the good lattice matching between the Ag(001) and Cr lattices, the enhanced surface energy of the Cr surface ($\sim$2400 mJ/m^2) compared to that of the Ag substrate ($\sim$1250 mJ/m^2) results in the Cr atoms being buried below a monolayer of Ag(001) [23]. Thus, the system forms a 1 ML Ag/1 ML Cr/Ag(001) [in short, 1 Ag/1 Cr/Ag(001)] sandwich structure. When expanded to the lattice constant of Ag(001), the magnetic moment on the Cr atoms in the freestanding monolayer is $4.45\mu_B$ per atom. Despite having Ag layers both above and below, the buried Cr monolayer still retains a large magnetic moment ($\sim$4.36μ_B), with the spins arranged in an AFM $c(2 \times 2)$ pattern [23]. The fact that the Cr layer retains, to a large extent, the greatly enhanced value of magnetic moment possessed by the freestanding monolayer, can be attributed to the relative absence of hybridization between the Ag $4d$ bands (whose center lies at comparatively low energy) and the Cr $3d$ states, leading to electronic isolation [15,19].

It is worth exploring and elucidating the detailed electronic structure of this system, as such studies on true two-dimensional (2D) AFM layer systems are rare in the literature. While some limited experimental data are available on the measured band dispersions of this system, using angle-resolved photoemission spectroscopy (ARPES), these experiments were performed more than a quarter of a century ago, using less sophisticated equipment than that currently available [26,32,37]. Further, they were compared to theoretically computed band structures, obtained using the tight-binding approximation [38], that moreover did not account for the Cr layer being buried under an Ag monolayer. In addition, earlier experimental and theoretical results contain limited information about band dispersions but not their intensities. It is therefore worth reexamining the electronic structure of this system, while making use of the more powerful experimental and theoretical tools available today.

Since these early experiments, photoemission spectroscopy has undergone revolutionary developments not only in terms of improved energetic and angular resolution, but also with the ability to detect low signal intensities and the capacity to collect data from large angular regions in parallel, with the help of 2D detectors. These technological advances allow one to reexamine the electronic structure of such interesting systems in far greater detail. In fact, our present photoemission results reveal the intriguing nature of the valence band dispersions of the Cr monolayer along different symmetry directions. At the same time, advances in the methodology of *ab initio* DFT calculations enable us to provide a more complete theoretical description of the electronic structure of the system.

In this paper, we have revisited the electronic and magnetic structure of a single monolayer of Cr deposited on an Ag(001) substrate, using a combination of ARPES experiments and spin-polarized DFT calculations. The unfolded band structure obtained from these calculations, along with appropriate spectral weight projections, has been compared with the experimentally measured band dispersions. We obtain good agreement between the theoretically computed and experimentally measured data for the band dispersions and intensities. Moreover, the calculations enable us to evaluate the contributions from different Ag and Cr layers and orbitals to each band as a function of wave vector; this enables us to obtain meaningful

insights that can be used to interpret the experimental ARPES results. Both our experiments and calculations show several weakly dispersive bands, which can be shown to arise primarily from the narrow $3d$ bands of the buried Cr atoms; they lie mostly within a window of 0–2 eV below the Fermi energy E_F. Substrate valence band features are absent within this range, except for the highly dispersive Ag sp bands. However, we also observe that near the zone edges, some of the Cr $3d$ bands display a strong dispersion; this has not been reported earlier.

The rest of this paper is organized as follows: In Sec. II, we give information about the experimental procedure followed for growth and deposition of our system and carrying out ARPES experiments. We also provide technical details regarding the computational methods used in the DFT calculations, and the procedure followed to "unfold" bands from the Brillouin zone of the supercell (corresponding to the magnetic structure) to the Brillouin zone of the primitive cell (corresponding to the chemical structure). In Sec. III, we present our results for the experimentally measured band dispersion, as obtained from ARPES, and compare them with the energies and intensities as computed from DFT. This also allows us to gain insight into the origin of the various features observed in the experimental ARPES data. In Sec. IV, we compare our results with those available previously in the literature, and also discuss further some interesting aspects of our results. Finally, we conclude in Sec. V with a brief summary of our main findings.

II. METHODS

A. Experimental details

A detailed description of the deposition and growth conditions for the monolayer of Cr on Ag(001), as well as the optimized values of various critical parameters, have been reported by us in a previous publication [35]. Briefly, Cr metal was deposited *in situ* from a water-cooled *e*-beam evaporator at a rate of 0.2 Å/min onto a clean and well-ordered Ag(001) substrate maintained at an elevated temperature of 428 K, with the chamber pressure maintained below 2×10^{-10} mbar during the deposition. The Cr monolayer was cooled down to room temperature (RT) immediately after deposition, to avoid the possible alloying of the film at elevated temperatures. Detailed low-energy electron diffraction (LEED) and photoelectron spectroscopy (PES) characterizations of the samples were performed to ascertain the structural and magnetic quality of the Cr film [23,35]. It should be noted that in our case, from the LEED experiment, we have extracted information not just about the geometric structure of the surface, but also about its magnetic structure, in particular, the fact that there is a $c(2 \times 2)$ antiferromagnetic ordering of the Cr spins. ARPES measurements were performed in the analysis chamber with base pressure better than 8×10^{-11} mbar and attached to the growth chamber, using a combination of VG SCIENTA-R4000WAL electron energy analyzer with 2D-CCD detector and a high-flux GAMMADATA VUV He lamp attached to a VUV monochromator; this has been described in detail elsewhere [39]. We used the He I$_\alpha$ (21.218 eV) and He II$_\alpha$ (40.81 eV) resonance lines to excite photoelectrons from the sample surface for the ARPES measurements, which were

performed at RT. The total experimental energy and angular resolutions were better than 100 meV and 1°, respectively, including the thermal broadening near E_F at RT. The reproducibility of all the results presented here was confirmed.

B. Computational details

All calculations were performed using spin-polarized DFT as implemented in the QUANTUM ESPRESSO package [40]. The interactions between the valence electrons and ionic cores were described using ultrasoft pseudopotentials [41]. The exchange-correlation functional was treated using a generalized gradient approximation of the Perdew-Burke-Ernzerhof form [42]. The wave functions and the corresponding charge densities were expanded in plane-wave basis sets with cutoffs of 40 and 400 Ry, respectively. It is worth mentioning here that we have also performed DFT+U [43] calculations with several different values of the Hubbard parameter (onsite Coulomb repulsion) U; we find that the results obtained with $U = 0$ match best with the experimental ARPES data. Therefore, in Sec. III B below, we have only presented the computational results corresponding to $U = 0$; this point is also discussed at greater length in Sec. IV further below.

To model the Ag(001) surface, we have considered a 21-atomic-layer-thick slab with a (1×1) surface unit cell. The use of a supercell becomes indispensable in DFT calculations when the crystal symmetry changes, e.g., due to AFM ordering as is the case here [see Fig. 1(a)]. Accordingly, for the antiferromagnetic (AFM) 1 Ag/1 Cr/Ag(001) system [see Fig. 1(a) for a top view], a symmetric 17-atomic-layer-thick slab with a $(\sqrt{2} \times \sqrt{2})$ surface unit cell was used, with Cr monolayers buried under both the top and bottom layers of

Ag; this surface unit cell contains two atoms per atomic layer as shown in Fig. 1(a). We note that slabs with such a large number of layers were required in order to avoid an interaction between the top and bottom surfaces of the slab, and a resulting splitting of the surface states. It was verified that the results obtained did not change upon increasing further the thickness of the slab. Henceforth, we refer to the (1×1) and the $(\sqrt{2} \times \sqrt{2})$ surface unit cells in real space as the primitive cell (PC) and supercell (SC), respectively, and the corresponding Brillouin zones in reciprocal space as the PBZ and SCBZ, respectively. For both Ag(001) and 1 Ag/1 Cr/Ag(001), the relative arrangement of layers was assumed to follow the ABAB... stacking sequence, which is characteristic of the face-centered-cubic (fcc) structure along the [001] direction.

With the increase in the supercell size for AFM 1 Ag/1 Cr/Ag(001) relative to the chemical unit cell, the size of the corresponding Brillouin zone (BZ) decreases. Thus, the first BZ corresponding to the supercell (SCBZ) [shown by the black dashed line in Fig. 1(b)] gets folded inside the first BZ corresponding to the primitive cell (PBZ) [shown by the black solid line in Fig. 1(b)]. Brillouin zone sampling was carried out using Monkhorst-Pack (MP) meshes [44] along with Marzari-Vanderbilt smearing [45] with a width of 0.001 Ry; the MP meshes were 17×17 for the PBZ for Ag(001) and 12×12 sampling for the SCBZ for 1 Ag/1 Cr/Ag(001), respectively.

The in-plane lattice constant for the Ag(001) surface [which is equal to $a(\mathrm{Ag})/\sqrt{2}$] was calculated to be 2.94 Å; this value is in good agreement with the previously reported theoretical value [46], as well as experiment. For both Ag(001) and 1 Ag/1 Cr/Ag(001), all atoms, except those belonging to the middle three layers of the slab, were allowed to relax using the Broyden-Fletcher-Goldfarb-Shanno (BFGS) algorithm, until the forces on these atoms were less than 0.001 Ry/bohr along each Cartesian direction.

C. Procedure for unfolding and projecting calculated band structure

The calculated bands in the SCBZ cannot be directly compared with the experimental ARPES data due to the folding of the SCBZ inside the PBZ; thus, they are not immediately sufficiently informative. In order to facilitate a direct comparison between the experiment and theory, an unfolding of the band structure corresponding to the (2×2) supercell in real space to the (1×1) cell in real space becomes essential. The theoretical formulation used for such an unfolding of bands has previously been given in Refs. [47–50]. Here, we present a summary regarding the implementation of such a methodology in a DFT plane-wave basis-set formulation.

Let us denote the wave vectors in the PBZ and SCBZ as $\mathbf{k}$ and $\mathbf{K}$, respectively, and the areas of the PBZ and SCBZ as Ω_{PBZ} and Ω_{SCBZ}, respectively. For each $\mathbf{K}$ of the SCBZ, there are $N_{\mathbf{G}}$ number of $\mathbf{G}^{\mathrm{SCBZ}}$ reciprocal lattice vectors corresponding to the AFM structure, that satisfy the following equation [51]:

$$\mathbf{k}_i = \mathbf{K} + \mathbf{G}_i^{\mathrm{SCBZ}} \quad \text{where} \quad i = 1 \ldots N_{\mathbf{G}}, \tag{1}$$

where $\mathbf{k}_i$ is any vector in the PBZ and $N_{\mathbf{G}} = \frac{\Omega_{\mathrm{PBZ}}}{\Omega_{\mathrm{SCBZ}}}$.
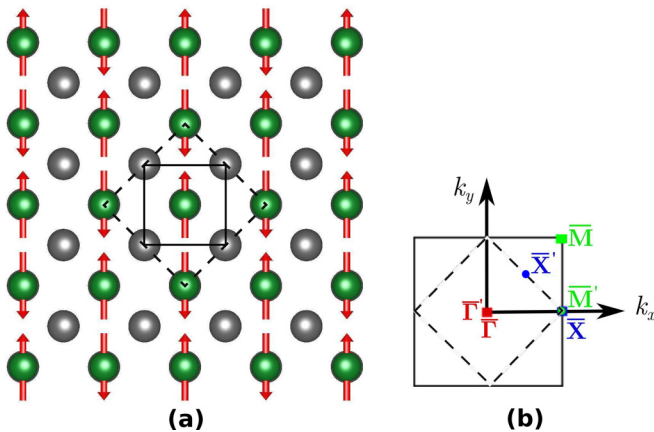
FIG. 1. Real and reciprocal space for 1 Ag/1 Cr/Ag(001). (a) Top view of the chemical and magnetic lattices in real space. The (collinear) spins are indicated by up and down arrows, and the Cr atoms in the second layer and Ag atoms in the topmost layer are represented by dark (green online) and gray spheres, respectively. The solid and dashed squares indicate the primitive cell (PC) of the chemical lattice and the $(\sqrt{2} \times \sqrt{2})$ supercell (SC) of the magnetic lattice, respectively. (b) The corresponding Brillouin zones in reciprocal space. The solid and dashed squares indicate the PBZ and the SCBZ, respectively (see text for description). The letters label high-symmetry points (unprimed letters are for the PBZ and primed letters are for the SCBZ).

Let us consider the single-particle Kohn-Sham (KS) states of the supercell $\psi_{\mathbf{K},m}^{SC}$; these can be obtained by solving the KS equations self-consistently by performing calculations using the supercell. When using a plane-wave basis, one can write

$$\left|\psi_{\mathbf{K},m}^{SC}\right\rangle = \sum_{\{\mathbf{G}^{SCBZ}\}} c_{\mathbf{K}-\mathbf{G}^{SCBZ},m}|\mathbf{K} - \mathbf{G}^{SCBZ}\rangle, \qquad (2)$$

where m is a band index, $|\mathbf{K} - \mathbf{G}^{SCBZ}\rangle$ represents the plane-wave basis functions, and $c_{\mathbf{K}-\mathbf{G}^{SCBZ},m}$ are the plane-wave expansion coefficients. Similarly, the single-particle KS states of the primitive cell for the chemical cell $\psi_{\mathbf{k},\nu}^{PC}$ are written as

$$\left|\psi_{\mathbf{k},\nu}^{PC}\right\rangle = \sum_{\{\mathbf{G}^{PBZ}\}} c_{\mathbf{k}-\mathbf{G}^{PBZ},\nu}|\mathbf{k} - \mathbf{G}^{PBZ}\rangle, \qquad (3)$$

where ν is the band index in the primitive cell. Note that the set of vectors $\{\mathbf{G}^{PBZ}\}$ is a subset of $\{\mathbf{G}^{SCBZ}\}$. Thus, Eq. (2) can be rewritten as

$$\left|\psi_{\mathbf{K},m}^{SC}\right\rangle = \sum_{\{\mathbf{G}^{PBZ}\}} c_{\mathbf{K}-\mathbf{G}^{PBZ},m}|\mathbf{K} - \mathbf{G}^{PBZ}\rangle$$
$$+ \sum_{\{\mathbf{G}^{SCBZ}\neq\mathbf{G}^{PBZ}\}} c_{\mathbf{K}-\mathbf{G}^{SCBZ},m}|\mathbf{K} - \mathbf{G}^{SCBZ}\rangle. \qquad (4)$$

As our aim is to obtain the right-hand side of Eq. (3) from Eq. (2), i.e., we want to obtain $\{\mathbf{G}^{PBZ}\}$ from the given set $\{\mathbf{G}^{SCBZ}\}$, we can employ the following condition:

$$\mathbf{G}^{SCBZ} \cdot \mathbf{A} = 2\pi M \quad \forall \{\mathbf{G}^{SCBZ}\}, \qquad (5)$$

where M is an integer and $\mathbf{A}$ is a lattice vector of the chemical structure. Equation (5) gives nonzero contributions only if $\mathbf{G}^{SCBZ} \in \{\mathbf{G}^{PBZ}\}$.

The probability of $|\psi_{\mathbf{K},m}^{SC}\rangle$ having the same character as a chemical structure state with wave vector $\mathbf{k}$ is given by the spectral weight $S_{\mathbf{K},m}(\mathbf{k})$. The spectral weight can then be obtained as [51]

$$S_{\mathbf{K},m}(\mathbf{k}) = \sum_{\nu} \left\langle \left|\psi_{\mathbf{K},m}^{SC}\right|\psi_{\mathbf{k},\nu}^{PC}\right\rangle \right|^2. \qquad (6)$$

As we are interested in obtaining the band structure in the PBZ, we can ignore the second term on the right-hand side of Eq. (4). Then, from Eqs. (3) and (4) we can write

$$S_{\mathbf{K},m}(\mathbf{k}) = \sum_{\{\mathbf{G}^{PBZ}\},\,\nu} |c_{\mathbf{K}-\mathbf{G}^{PBZ},m}|^4 \delta_{m\nu}. \qquad (7)$$

To obtain the contributions coming from individual atomic states to the bands, one can write $\psi_{\mathbf{K},m}^{SC}$ as

$$\psi_{\mathbf{K},m}^{SC} = \sum_{q} A_q \phi_q, \qquad (8)$$

where $\{q\}$ is the set of good quantum numbers. ϕ_q is the atomic orbital corresponding to the state q and the A_q's are the corresponding coefficients. The probability of the wave function $\psi_{\mathbf{K},m}^{SC}$ having the same character as an orbital ϕ_q is

given by

$$\left|\langle\phi_q|\psi_{\mathbf{K},m}^{SC}\rangle\right|^2 = |A_q|^2. \qquad (9)$$

Note that here we have assumed that all the calculations are performed in the supercell.

Now, to obtain the contributions coming from the atomic states to the unfolded bands, one has to calculate the probability of the wave function $\psi_{\mathbf{k},\nu}^{PC}$ having the same character as an orbital ϕ_q, i.e., the projected spectral weight P, which can be written as

$$P = \left|\langle\phi_q|\psi_{\mathbf{k},\nu}^{PC}\rangle\right|^2 = \left|\langle\phi_q|\psi_{\mathbf{K},m}^{SC}\rangle\langle\psi_{\mathbf{K},m}^{SC}|\psi_{\mathbf{k},\nu}^{PC}\rangle\right|^2 \qquad (10)$$
$$= |A_q|^2 \, S_{\mathbf{K},\nu}(\mathbf{k}).$$

P is a very useful quantity, enabling one to extract the rich physics of the system, which is buried in the folded band structure. In Sec. III B, P has been used to compare the ARPES data of both Ag(001) and Ag/Cr/Ag(001) with the theoretically obtained band structure. We note that $S(k)$ is zero for the Ag(001) surface as no supercell is required for the system; therefore, P indicates only the projected band structure in that case.

III. RESULTS

A. Experimental results

In this section, we present experimental data obtained using ARPES. Figures 2(a) and 2(b) show ARPES data obtained from the clean Ag(001) substrate along the $\overline{\Gamma}$ to $\overline{X}$ and $\overline{\Gamma}$ to $\overline{M}$ symmetry directions, respectively. Monochromatic He I$_\alpha$ photons were used to probe the valence band electronic
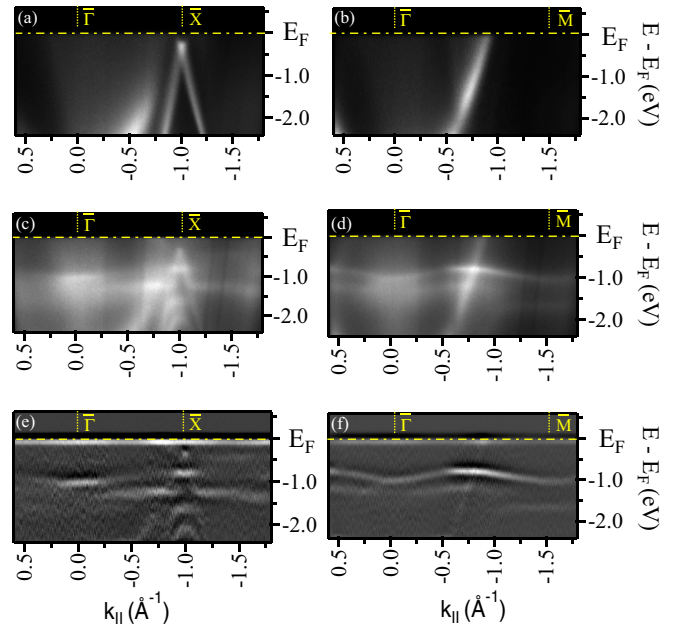
FIG. 2. ARPES data from clean Ag(001) substrate using He I$_\alpha$ photons along (a) $\overline{\Gamma}$ to $\overline{X}$ and (b) $\overline{\Gamma}$ to $\overline{M}$ directions. ARPES data from 1 Ag/1 Cr/Ag(001) sandwich layers along (c) $\overline{\Gamma}$ to $\overline{X}$ and (d) $\overline{\Gamma}$ to $\overline{M}$. 2D second derivative of the ARPES data in (c) and (d) are shown in figures (e) and (f), respectively, where the band dispersions are more clearly visible.

structure in the range from 0 to -2.4 eV in the energy scale of $E - E_F$. Since the intense Ag d states are found at much lower energies (~ 4 eV below E_F), the only bands visible within this energy window are the highly dispersive Ag sp states [52–57].

Figures 2(c) and 2(d) show the ARPES data obtained from a 1 Ag/1 Cr/Ag(001) sample along the $\overline{\Gamma}$-$\overline{X}$ and $\overline{\Gamma}$-$\overline{M}$ symmetry directions, respectively, using He I$_\alpha$ photons at RT. Along both these directions, we observe low-intensity features within the energy window considered; a comparison with Figs. 2(a) and 2(b) shows that deposition of the monolayer of Cr has resulted in a drastic change in the ARPES data. In Figs. 2(e) and 2(f), the intensity plot of the 2D second derivative [58] of the ARPES data of Figs. 2(c) and 2(d) is shown, which provides a better way of visualizing these weakly dispersive features. Note that here the intense flat feature just below E_F is an artifact resulting from the second derivative of the Fermi edge. Interestingly, no bands are found to cross E_F along both the symmetry directions shown in Fig. 2 as well as along other directions within the surface Brillouin zone (not shown here). However, this need not necessarily indicate the existence of a hard energy gap between the occupied and unoccupied bands as the presence of weak and featureless intensity near E_F could be due to the Cr ds states or from the Ag sp states.

The observed bands are found to be only weakly dispersive throughout the surface Brillouin zone, except near the $\overline{X}$ and $\overline{M}$ points. Near the $\overline{X}$ point, two bands with large negative curvature are observed, with energies of -1.6 eV and -2.0 eV at $\overline{X}$, respectively. The intensity of these strongly dispersive features [see Fig. 2(e)] appears to be modulated by the presence of Ag sp bands. Near the $\overline{M}$ point, a flat band at -1.7 eV energy can be observed, with a negative curvature below -1.2 Å^{-1} [see Fig. 2(f)]. The dispersive nature of this band, as well as a similarly dispersive band at lower energy, can be more clearly observed in the ARPES data using He II$_\alpha$ photons, as will be demonstrated further below.

In the energy window where $E - E_F > -1.5$ eV, the band structure prominently features two weakly dispersive bands with a bandwidth of about 250 meV along both the $\overline{\Gamma}$-$\overline{X}$ and $\overline{\Gamma}$-$\overline{M}$ directions, though the band dispersion along $\overline{\Gamma}$-$\overline{M}$ is relatively higher. At $\overline{\Gamma}$, these bands are at -1.05 and -1.35 eV, respectively, and along the $\overline{\Gamma}$-$\overline{X}$ direction, they reach the highest $E - E_F$ value at the $\overline{X}$ point. For the $\overline{\Gamma}$-$\overline{M}$ direction, these bands reach the highest $E - E_F$ value at the midpoint along $\overline{\Gamma}$-$\overline{M}$, and have roughly the same energy (-1.05 eV) at the $\overline{\Gamma}$ and $\overline{M}$ points. This suggests that the system may have a $c(2 \times 2)$ symmetry, rather than the $p(1 \times 1)$ symmetry of the chemical unit cell [see Fig. 1(b)]. This is also compatible with the $c(2 \times 2)$ symmetry observed previously by the magnetically exchange-scattered electrons as measured in the low-energy electron diffraction (LEED) pattern, which we had shown results from a $c(2 \times 2)$ antiferromagnetic alignment of the spins in the buried Cr monolayer [23]. (Note that as a result of the antiferromagnetism of the Cr lattice and the folding of the BZ, the $\overline{M}$ point of the PBZ becomes the $\overline{\Gamma}'$ point of the SCBZ. However, in order to avoid confusion and for better comparison, we continue to refer all the high-symmetry points in the ARPES data with respect to the PBZ.) The intensity of these bands is also found to vary through the Brillouin zone. Along $\overline{\Gamma}$-$\overline{X}$, the band closest to E_F is found to have high
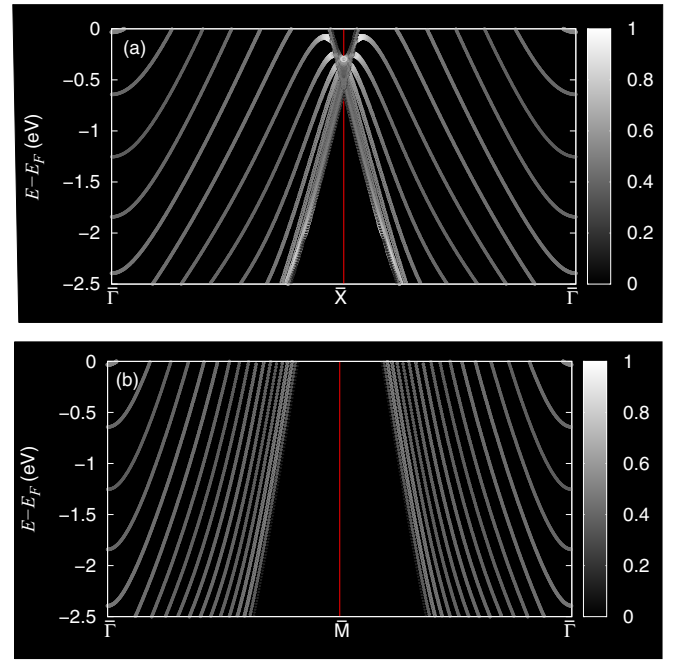
FIG. 3. Theoretically computed results from DFT for the electronic band structure of the bare Ag(001) surface, along the (a) $\overline{\Gamma}$-$\overline{X}$-$\overline{\Gamma}$ and (b) $\overline{\Gamma}$-$\overline{M}$-$\overline{\Gamma}$ directions. The gray color scale represents the value of the projection P (see text for the definition).

intensities in the vicinity of the $\overline{\Gamma}$ and $\overline{X}$ points, while along $\overline{\Gamma}$-$\overline{M}$, the maximum intensity is observed near the midpoint [the $\overline{X}'$ point, see Fig. 1(b)]. The second-lowest-energy band is only barely visible at the $\overline{\Gamma}$, $\overline{X}$, and $\overline{M}$ points. We also observe a low-intensity band with weak dispersion at -0.45 eV, beyond the $\overline{X}$ point [see Fig. 2(e)]. A careful observation reveals a faint-intensity counterpart of this band at $\overline{\Gamma}$ point also. This will be further discussed in Sec. IV.

B. Theoretical results

In order to better understand the electronic structure of this system, we have carried out DFT calculations on a realistic model of the system, consisting of 1 Ag/1 Cr/Ag(001), with a $c(2 \times 2)$ unit cell, with AFM alignment of the Cr spins. In previous work, we had shown that this is the ground-state geometric and magnetic configuration for this system [23]. Here, we are particularly interested in obtaining band structures that can be compared with the ARPES spectra, and in exploring the existence of possible electronic hybridization effects between the Cr and Ag states.

We first compute the electronic band structure of the bare Ag(001) surface (see Fig. 3), along two different high-symmetry directions of the primitive Brillouin zone, viz., $\overline{\Gamma}$-$\overline{X}$-$\overline{\Gamma}$ and $\overline{\Gamma}$-$\overline{M}$-$\overline{\Gamma}$. Since ARPES probes the surface electronic structure, we have projected the calculated band dispersions onto the orbitals of the atoms belonging to the four outermost Ag layers on both sides of the slab. In Fig. 3, the gray scale represents the extent of overlap P between the Kohn-Sham state and the relevant atomic orbitals, as given by Eq. (10); here "white" color represents bands with the highest amount of overlap P, while "black" color represents bands with $P = 0$.

As we have used the primitive cell of the chemical lattice for the DFT calculations of the bare Ag(001) surface (Ag being nonmagnetic), no unfolding is required in this case.

We have compared our results with the corresponding ARPES data for the bare Ag(001) surface shown in Figs. 2(a) and 2(b). We find that the calculated and experimental band structures are in good agreement. In particular, the computed and the experimentally measured binding energies agree near the red vertical lines marked in Fig. 3, which pass though either the $\overline{X}$ or $\overline{M}$ points. Away from these lines, we observe the presence of a finite number of discrete states with nonzero P in our calculated band dispersions, because of the finite thickness of the slab. In a real experimental scenario, because of the very large thickness of the slab, we will actually have a diffuse continuum of states in this energy range. We also note that (except of course for the number of projections of bulklike states) our calculated dispersions are found to be converged with respect to the thickness of the slab.

Next, we proceed to calculate the band structure of 1 Ag/1 Cr/Ag(001). In this case, the unfolding of the band structure from the SCBZ [shown by the dashed black lines and high-symmetry points $\overline{\Gamma'}$, $\overline{X'}$, and $\overline{M'}$ in Fig. 1(b)] to the PBZ [shown by the solid black lines and high-symmetry points $\overline{\Gamma}$, $\overline{X}$, and $\overline{M}$ in Fig. 1(b)] is necessary as one cannot define an antiferromagnetic configuration in the primitive (chemical) unit cell. Moreover, as expected from the antiferromagnetic interactions between the neighboring Cr atoms, the bands corresponding to the spin up and spin down are always found to be degenerate.

Figures 4(a) and 4(b) contain our results along the $\overline{\Gamma}$-$\overline{X}$-$\overline{\Gamma}$ and $\overline{\Gamma}$-$\overline{M}$-$\overline{\Gamma}$ directions, respectively. In these figures, the
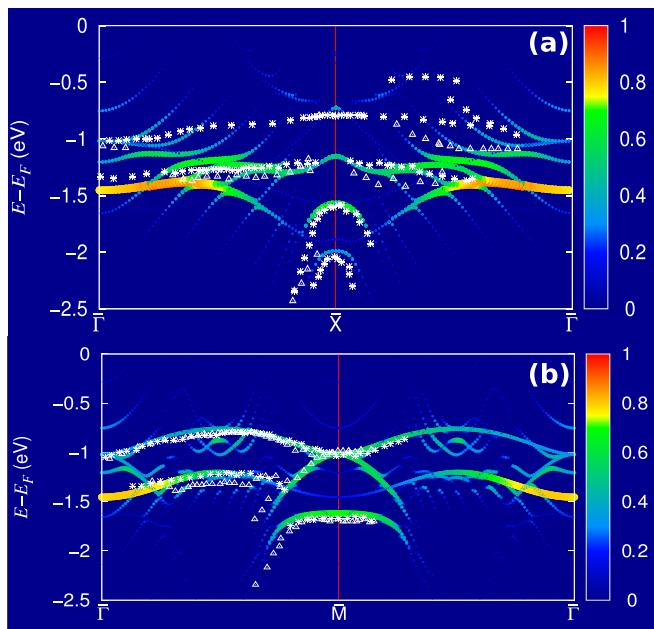
color scale is used to represent the value of the theoretically computed projection P as defined in Eq. (10), where "red" color represents the bands with the highest value of P, and "dark blue" color represents the bands with zero P. While calculating P, we have obtained the value of A_q [see Eq. (9)] by projecting onto the orbitals of the atoms belonging to the first two surface layers of the 1 Ag/1 Cr/Ag(001) slab. No significant modification was observed upon considering more layers for projection. The experimental data from ARPES are also plotted on these figures, with the white stars and open triangles representing He I$_\alpha$ and He II$_\alpha$ data, respectively. We see from Fig. 4 that we get excellent agreement between the experimentally measured ARPES data and the calculated band dispersions and intensities.

Earlier, upon comparing the ARPES data for Ag(001) and 1 Ag/1 Cr/Ag(001), it was obvious that several additional states appear at the $\overline{X}$ point due to the presence of Cr atoms. Similarly, here, upon comparing Fig. 3 for bare Ag(001) with Fig. 4 for 1 Ag/1 Cr/Ag(001), we find that several new states have arisen due to the introduction of the buried Cr layer. On further decomposing P so as to separate out the contributions from various orbitals of the Cr atoms [see Figs. 5(a)–5(j)], we find that these states originate primarily from the Cr 3d orbitals. We have labeled these additional states at $\overline{X}$ as Si_X, where i = 1–5. These states have band edges at $E - E_F = -1.98$ eV, -1.57 eV, -1.57 eV, -0.72 eV, and -1.15 eV, and arise from the five Cr 3d orbitals: 3d_{xy}, 3d_{yz}, 3d_{zx}, 3$d_{x^2-y^2}$, and 3d_{z^2}, respectively. We find that the states arising from 3d_{yz} and 3d_{zx}, i.e., $S2_X$ and $S3_X$ are degenerate; this is due to the fact that the surface of the slab is perpendicular to the z direction in our calculation.

In Fig. 6, we have plotted the electronic charge density profiles for each of these "new" Cr-induced states, for an isosurface value of 0.001 e/a.u.^{3} for one of the two degenerate spin channels; for the other spin channel one can obtain similar charge density profiles by interchanging the states corresponding to the two Cr atoms (shown by green spheres in Fig. 6) in the supercell. We see that the charge densities for all the five states are mainly localized on the Cr atoms, as one might have expected from the projected band structure calculations. Moreover, we see that the charge densities decay as one moves away from the Cr layer, both into the bulk and toward the surface [see Figs. 6(f)–6(j)].

Similarly, on comparing Figs. 3(b) and 4(b), we find several additional states appear in 1 Ag/1 Cr/Ag(001) at the $\overline{M}$ point. We have denoted these states at $\overline{M}$ as Si_M, where i = 1–4. These states have band edges at $E - E_F = -1.45$ eV, -1.02 eV, -1.02 eV, and -1.65 eV and arise from the four Cr 3d orbitals: 3d_{xy}, 3d_{yz}, 3d_{zx}, and 3$d_{x^2-y^2}$, respectively. This can be seen from Figs. 5(f)–5(j) where we have replotted the individual orbital-decomposed contributions to the band dispersion along $\overline{\Gamma}$-$\overline{M}$. We find the states arising from 3d_{yz} and 3d_{zx}, i.e., $S2_M$ and $S3_M$, are again degenerate at $\overline{M}$. Note that there is no perceptible intensity from 3d_{z^2} states at $\overline{M}$. In Fig. 7, we have shown the electronic charge density profiles for each of these surface states at $\overline{M}$, for an isosurface value of 0.001 e/a.u.^{3} for one spin channel. In this case also, we find that the charge densities are mostly localized on the Cr atoms and decay rapidly away from the Cr layer.

FIG. 4. Theoretically computed results from DFT for the projected unfolded band structure of 1 Ag/1 Cr/Ag(001) along the (a) $\overline{\Gamma}$-$\overline{X}$-$\overline{\Gamma}$ and (b) $\overline{\Gamma}$-$\overline{M}$-$\overline{\Gamma}$ directions. The color scale represents the projected spectral function P (see text for definition). The white stars and open triangles represent the experimental ARPES data using He I$_\alpha$ and He II$_\alpha$ photons, respectively.
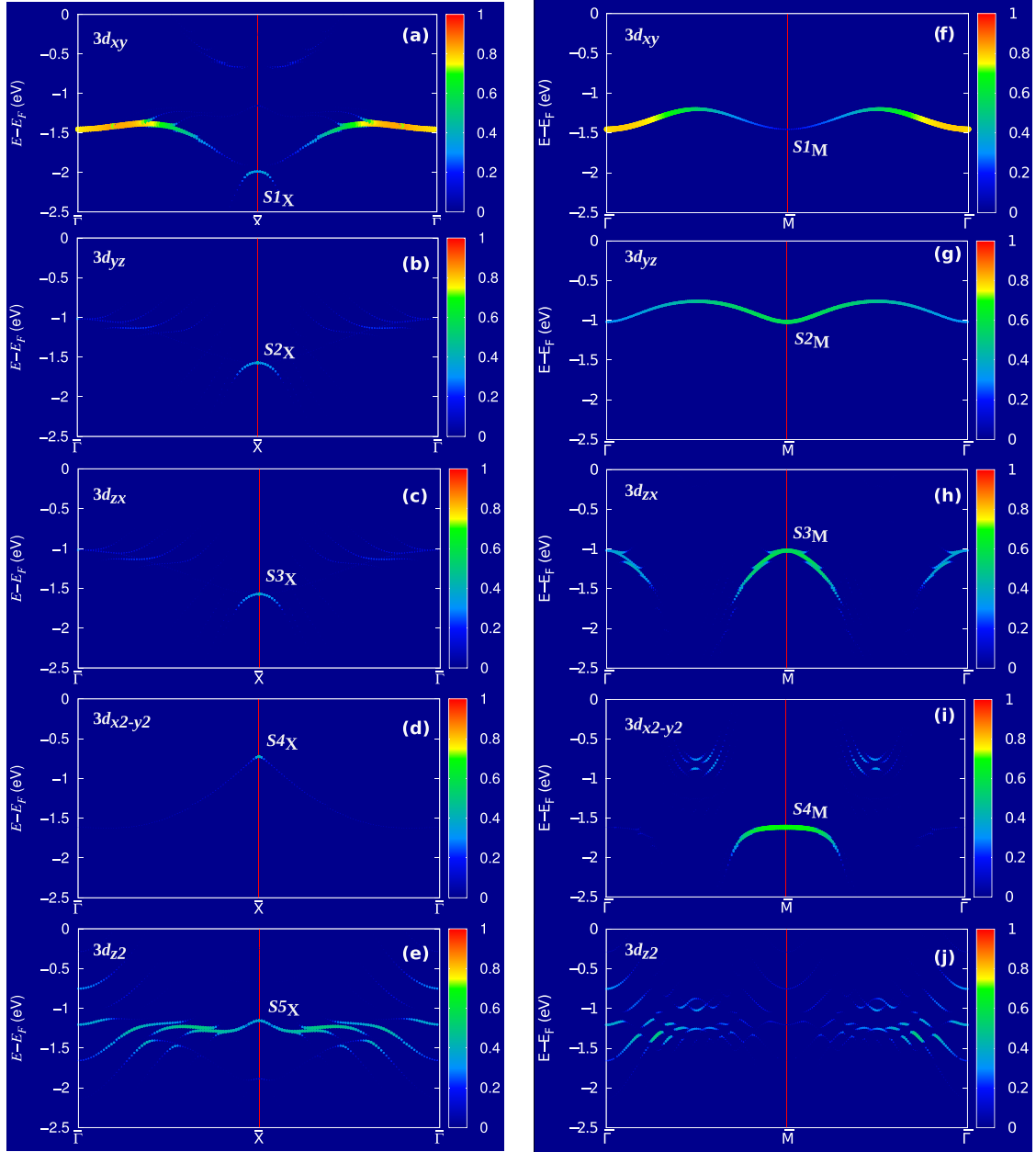
FIG. 5. Theoretically computed results from DFT for orbital-projected unfolded band structure of 1 Ag/1 Cr/Ag(001) along (a)–(e) $\overline{\Gamma}$-$\overline{X}$-$\overline{\Gamma}$ and along (f)–(j) $\overline{\Gamma}$-$\overline{M}$-$\overline{\Gamma}$ on the five individual Cr 3d states, i.e., $3d_{xy}$, $3d_{yz}$, $3d_{zx}$, $3d_{x^2-y^2}$, and $3d_{z^2}$, respectively. The color scale represents the projected spectral function P (see text for definition).

It is noteworthy that the calculated band structure shown in Fig. 4 for 1 Ag/1 Cr/Ag(001) is in excellent agreement with the ARPES data. While comparing the intensities of the theoretically computed and experimentally measured bands in Figs. 2 and 4, we find that the overall agreement between the calculated band structure and ARPES data is very good, with the exception of the $S4_X$ state (with band edge at -0.72 eV). The intensity of this state at $\overline{X}$ appears to be rather high in the experimental data; however, we do not observe such a high intensity for this state in the calculated band structure. We have verified that the computed intensity of the $S4_X$ feature does not change appreciably upon taking into account also the projections from the Ag layers which are below the Cr layer.

This once again confirms that $S4_X$, along with the other states, originates solely from the Cr atoms. As earlier experimental results [23,35,59] suggest that some degree of intermixing of Ag and Cr is possible, it may be that the high intensity of $S4_X$ in the experimental data arises from the presence of some Cr atoms in the topmost surface layer, due to intermixing.

IV. DISCUSSION

We first compare our results with those of previous authors. Although the ARPES data reported in this study are, to some extent, in qualitative agreement with previous measurements reported in the literature [26,32], there are important differ-
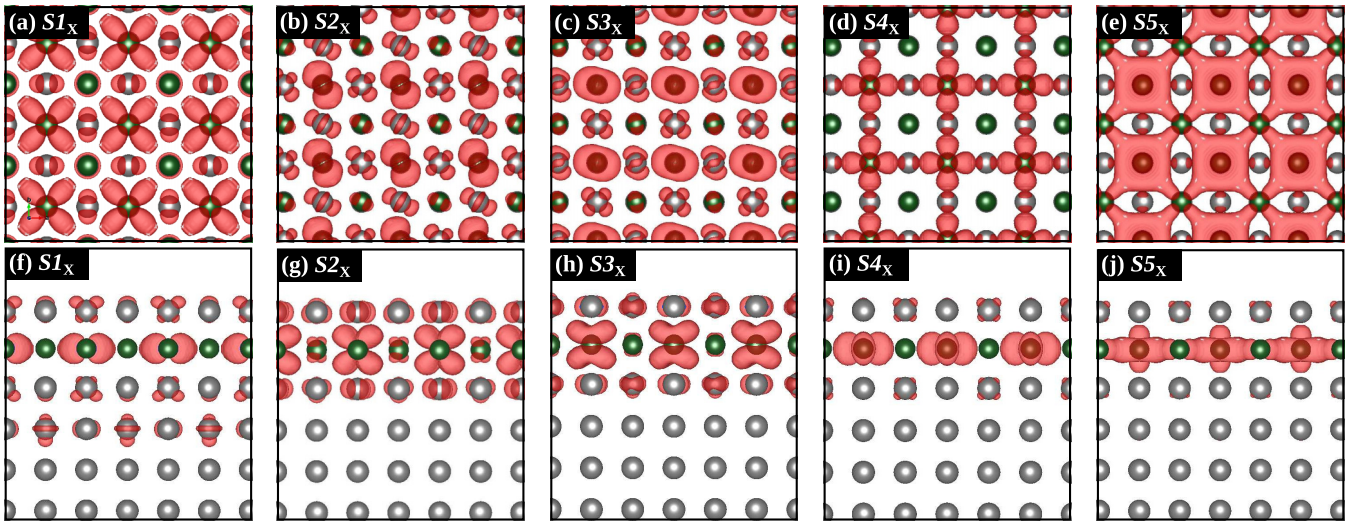
FIG. 6. Band-resolved charge density profiles as computed from DFT, for AFM 1 Ag/1 Cr/Ag(001). The top [(a)–(e)] and side [(f)–(j)] views of the charge density profiles (red) for one spin channel, corresponding to the "surface states" at $\overline{X}$. The top views correspond to the x-y plane, while the side views correspond to either the y-z or the z-x plane. The green and the gray spheres represent the Cr and Ag atoms, respectively. The isosurface value for the charge density is 0.001 e/a.u^3.

ences (both qualitative and quantitative) between our results and those of previous authors. The highly dispersive states observed by us near the $\overline{X}$ and $\overline{M}$ points have not been reported in these previous studies. However, the previous studies reported another weakly dispersive band at around 1.75 eV below E_F, along both the $\overline{\Gamma}$-$\overline{X}$ and $\overline{\Gamma}$-$\overline{M}$ directions; this band has not been observed by us in our ARPES experiments, nor does it appear in our computed DFT band structure. We believe that these differences can be attributed to the superior experimental conditions prevailing in this work, including the use of a monochromatized high-intensity photon source and a high-transmission electron energy analyzer with 2D-CCD detector, enabling accurate band assignments, despite the weak intensity of some of the observed bands.

Our computed band structure also differs from that obtained in a previous theoretical study [38]. The agreement between experimental data and the computed band structure obtained in the previous study is not particularly satisfactory. There is some degree of matching only for the lowest band, that too only along $\overline{\Gamma}$-$\overline{M}$ and not along $\overline{\Gamma}$-$\overline{X}$. The earlier computations do not reproduce the bands observed at about -1.5 eV below E_F, nor do they yield the additional states near the $\overline{X}$ and $\overline{M}$ points. We believe that the main source of discrepancy with experiment is that these earlier computations were performed for the 1 Cr/Ag(001) system and not the 1 Ag/1 Cr/Ag(001) system; moreover, the method used previously was the less accurate tight-binding approximation, rather than first-principles DFT as in this study.
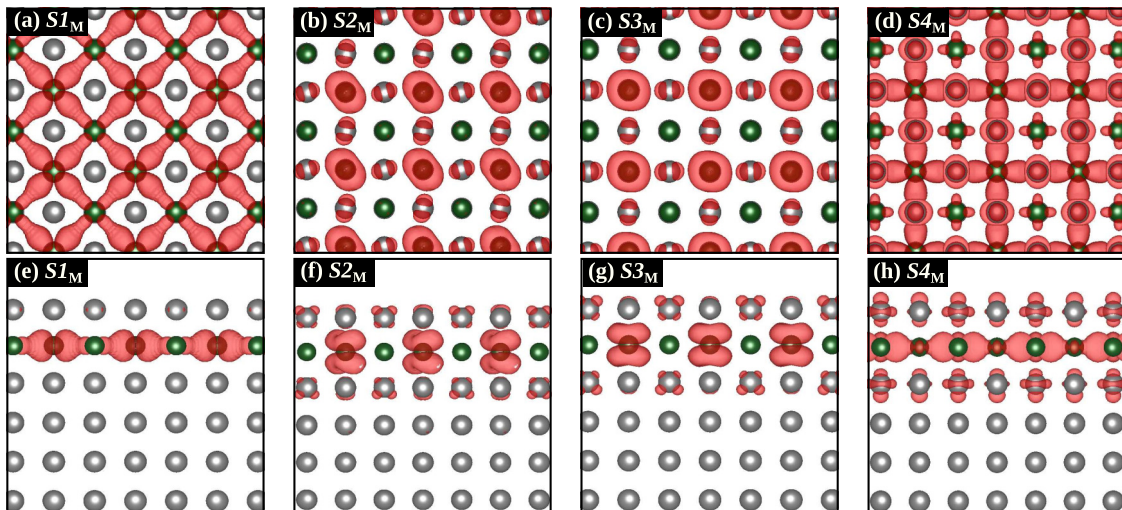
FIG. 7. Band-resolved charge density profiles as computed from DFT for AFM 1 Ag/1 Cr/Ag(001). The top [(a)–(d)] and side [(e)–(h)] views of charge density profiles (red), for one spin channel, corresponding to the "surface states" at $\overline{M}$. The top views correspond to the x-y plane, while the side views correspond to either the y-z or the z-x plane. The green and the gray spheres represent the Cr and the gray spheres represent the Cr and Ag atoms, respectively. The plots depict the isosurface for 0.001 e/a.u^3.

It should be noted that the highly dispersive states observed in the ARPES data below -1.0 eV binding energy around the $\overline{X}$ and $\overline{M}$ symmetry points (see Fig. 2) are in fact the quantum-well (QW) states formed within the Cr monolayer in 1 Ag/1 Cr/Ag(001) system due to the electron confinement. As the Ag band structure displays an energy gap at both the $\overline{M}$ and $\overline{X}$ points (see Fig. 3), in these regions the Cr $3d$ electrons are reflected back by the Ag barriers on either side, resulting in the formation of these QW states with parabolic dispersions. These d-band QW states also display the characteristic negative-curvature dispersions, as observed in other d-band QW systems [60,61]. Our DFT calculations also correctly predict their binding energy positions as well as the nature of their dispersions (see Figs. 4 and 5). The charge density plots (see Figs. 6 and 7) also show that these states are localized primarily on the Cr layer. Here, we obtain two different QW states for the Cr monolayer as there are two Cr $3d$ bands crossing the Ag band-gap region.

By comparing the ARPES results obtained using He I$_\alpha$ and He II$_\alpha$ photons (see the stars and open triangles in Fig. 4) it is also observed that the two sets of data coincide in energy, implying that these bands have negligible dispersion along the k_z direction. This provides evidence in favor of the true two-dimensional character of the Cr $3d$ bands, and supports the presence of a flat monolayer of Cr, without any significant agglomeration or island formation.

We have mentioned above that the states observed in ARPES for 1 Ag/1 Cr/Ag(001) arise primarily from the Cr $3d$ states. However, the presence of Ag atoms in the overlayer and substrate does affect the electronic structure. In order to examine this issue, it is instructive to compare the theoretical results obtained for 1 Ag/1 Cr/Ag(001) with those computed for a freestanding monolayer of Cr atoms. Accordingly, we consider a single monolayer of Cr atoms arranged in a square lattice, with the lattice constant fixed at that of the supercell (see Sec. II B), with the spins aligned antiferromagnetically in the same $c(2 \times 2)$ arrangement. As already mentioned, we find the magnetic moment on each Cr atom in this case is $4.46\mu_B$ whereas for the buried Cr monolayer in 1 Ag/1 Cr/Ag(001), the moments on the Cr atoms are $4.36\mu_B$ [23]. In Figs. 8(a) and 8(b) we have plotted the projected unfolded band structure for this system along the $\overline{\Gamma}$-$\overline{X}$-$\overline{\Gamma}$ and $\overline{\Gamma}$-$\overline{M}$-$\overline{\Gamma}$ directions. As in Fig. 4 above, the color scale in this figure represents the projected spectral weight P. From Fig. 8(b), we see that there is a gap at the Fermi level along $\overline{\Gamma}$-$\overline{M}$-$\overline{\Gamma}$; in contrast, we see from Fig. 8(a) that there is "semimetal-like" behavior along $\overline{\Gamma}$-$\overline{X}$-$\overline{\Gamma}$, with the bands touching E_F only at two points near $\overline{X}$. Upon deposition on Ag(001), together with being buried under a monolayer of Ag atoms, we see, by comparing the results in Figs. 4 and 8 that the bands change in three main ways: (i) the Cr bands are comparatively pushed down in energy because of the Fermi level being raised by the Ag states, (ii) the strongly dispersive bands with negative curvature in the neighborhood of the $\overline{X}$ and $\overline{M}$ points become more prominent, (iii) the relative intensity of the flat Cr $3d$ bands is flipped; in the freestanding monolayer, the bands that arise from the Cr $3d_{xy}$ states are more intense than those that arise from the $3d_{xz}$ and $3d_{yz}$ states; in 1 Ag/1 Cr/Ag(001) the situation is reversed, due to the Cr $3d$ electrons being sandwiched between Ag atoms.
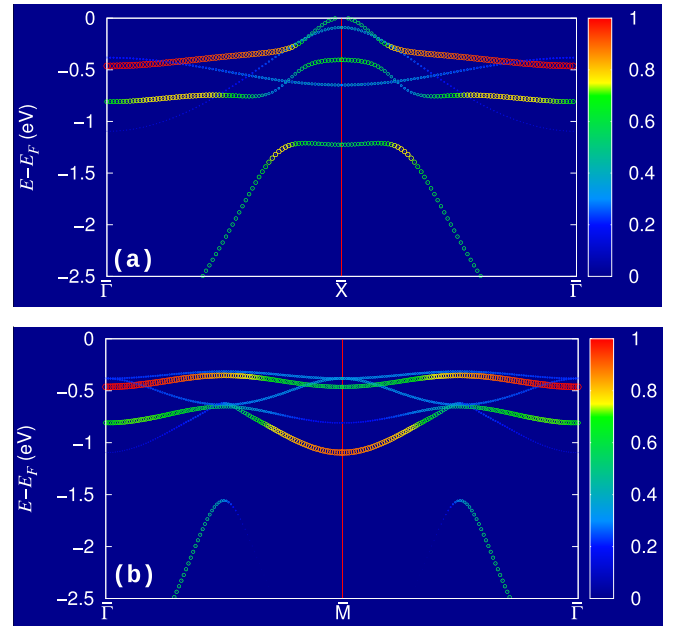
FIG. 8. Theoretically computed results from DFT for the projected unfolded band structure of a freestanding antiferromagnetic Cr monolayer [with lattice constant set equal to that of Ag(001)] along the (a) $\overline{\Gamma}$-$\overline{X}$-$\overline{\Gamma}$ and (b) $\overline{\Gamma}$-$\overline{M}$-$\overline{\Gamma}$ directions. The color scale represents the projected spectral function P (see text for definition). It is instructive to compare these results with those in Fig. 4.

In Fig. 9 we have plotted the projected density of states (PDOS) of (a) the Cr $3d$ states for the freestanding Cr monolayer, (b) the Cr $3d$ states in 1 Ag/1 Cr/Ag(001), and (c) the Ag $4d$ and $5s$ states in 1 Ag/1 Cr/Ag(001). These graphs show that although there is very little overlap between the PDOS of Ag and Cr in 1 Ag/1 Cr/Ag(001), the PDOS (and hence, the band dispersions) of Cr are altered not just in energy but also in shape on embedding the Cr monolayer within the Ag slab. The fact that the Cr $3d$ orbitals are primarily responsible for the observed ARPES data can easily be attributed to the significantly higher PDOS of the Cr $3d$ states in the energy range of interest (i.e., -2.5 eV $< E - E_F < 0$ eV), compared to the PDOS of the Ag states and the Cr $4s$ states. However, there is still some hybridization between the Cr $3d$ states and the Ag states. In particular, we find that on going from the freestanding Cr monolayer to the embedded Cr monolayer in 1 Ag/1 Cr/Ag(001), there is a significant broadening of the bandwidth of the Cr $3d_{xz}$ and $3d_{yz}$ states, due to hybridization with the Ag states in the layers above and below. Interestingly, at the same time, we also find that the bandwidth of the Cr $3d_{xy}$ states reduces on going from the freestanding monolayer to the sandwich system, suggesting that there is charge redistribution within the Cr plane. However, we do not find any net charge transfer between the Cr and Ag atoms, despite the difference in electronegativitity between the two species.

As already mentioned in Sec. II B above, we had found, when performing our DFT computations, that introducing an onsite Coulomb interaction U on the Cr sites did not improve the agreement between theory and experiment. On the contrary, with increasing value of U, the agreement worsened. We found that the states below E_F are pushed down in energy to an ever
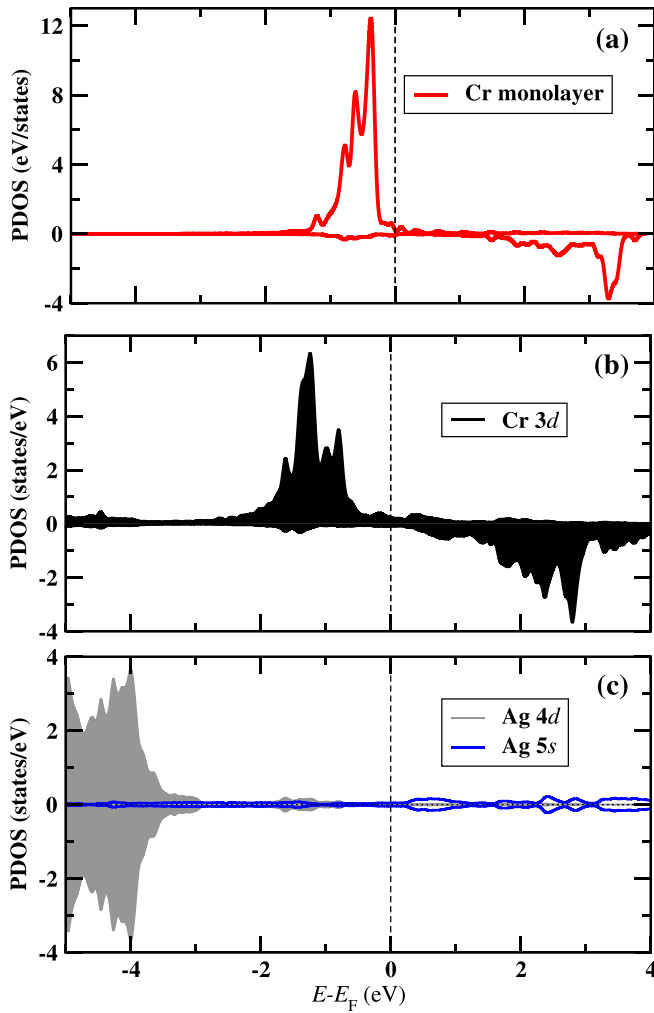
FIG. 9. Projected densities of states (PDOS) as calculated from DFT. (a) The Cr 3d states for the freestanding Cr monolayer, (b) the Cr 3d states in 1 Ag/1 Cr/Ag(001), and (c) the topmost layer Ag 4d and 5s states in 1 Ag/1 Cr/Ag(001).

greater extent, upon increasing the value of U, thereby progressively increasing the discrepancy between the experimentally measured and theoretically computed band dispersion curves. We therefore conclude that for the 1 Ag/1 Cr/Ag(001) system, the appropriate value of the onsite Coulomb interaction is $U \approx 0$. We note that the appropriate value of U for Cr in chromium oxides, for example, is of the order of 4 eV [62]. In the case of metals, it is known that the effective value of U decreases due to the screening by the delocalized electrons. Thus, for example, in the case of elemental metallic Cr, the value of U was estimated to be around 2 eV [63]. In the present case, where a monolayer of Cr is sandwiched between Ag layers, the screening is further enhanced due to the sp electrons of Ag, thereby further reducing the effective value of U, bringing it down close to zero. Thus, despite the observed narrow bandwidth of the Cr d bands (about 250 meV), we find that the 1 Ag/1 Cr/Ag(001) system behaves like a weakly correlated metal, due to enhanced screening effects, despite previous suggestions in the literature that it may be a strongly correlated system [32].

Further, it is interesting to note that for the 1 Ag/1 Cr/Ag(001) system, we do not observe any Cr 3d bands crossing the E_F in the experimental ARPES data (see Fig. 2), consistent with the previous experimental studies [26,32]. In our calculated band structure, though there is indeed a band crossing observed at the Fermi energy [see Figs. 4 and 5(a)], these features have low intensity and are therefore not clearly visible. However, our computed densities of states show the existence of a finite density of Cr 3d states at E_F (see Fig. 9), suggesting the absence of any hard gap in the system. It is possible that the failure to observe any band crossing at E_F is due to the limitations of the experimental setup and further experiments using advanced synchrotron facilities could resolve this issue. Normally, an antiferromagnetic ground state favors an insulating behavior, however, in the present case, the Cr monolayer still remains an itinerant d metal, possibly due to its weak electron correlation nature (low U/W value), where W is the bandwidth.

Finally, we note that upon varying the Cr coverage between 0.5 and 1.5 ML, we have not observed any perceptible changes in the measured band dispersion, though the intensity of the bands is found to scale with the Cr coverage [23]. We obtained maximum intensity of the Cr 3d bands at 1.2 ML Cr coverage, instead of the expected single ML coverage which has been attributed to the inevitable $\sim$20% intermixing between the Cr and top-layer Ag atoms during growth at 428 K [23,59]. This intermixing results in positional exchange of atomic species which leaves a few Cr atoms uncovered at the topmost Ag layer. The low-intensity band feature observed in the ARPES spectra at binding energy of -0.45 eV beyond $\overline{X}$ and around $\overline{\Gamma}$ [see Figs. 2(e) and 4(a)], which are not reproduced by the DFT calculations are expected to be contributed by these bare Cr atoms at the top surface layer.

V. SUMMARY AND CONCLUSIONS

In summary, we have performed a combined experimental and theoretical study of the electronic structure of a monolayer of Cr deposited on the Ag(001) surface. In earlier work [23], we had found, in agreement with previous studies [26,32], that the moments on the Cr atoms become antiferromagnetically aligned in a $c(2 \times 2)$ pattern; we had also demonstrated that the Cr monolayer is buried under one layer of Ag atoms, resulting in a 1 Ag/1 Cr/Ag(001) system. Here, we have measured the electronic structure of this system using ARPES, and compared it with the computed band structure obtained using DFT.

We find very good agreement between our experimental and theoretical results, regarding both the dispersions of the bands and their intensities. We observe two weakly dispersive bands that had also been reported by previous authors. In addition, we also observe several additional bands, including some with strongly negative curvature, in the vicinity of the $\overline{X}$ and $\overline{M}$ points. The origin of these features can be attributed to the formation of quantum well states arising from Cr d states that cross the bulk band-gap region of the surface-projected band structure of Ag(001); these states are reflected back by the Ag atoms on either side of the embedded Cr layer. Thus, despite the lack of overlap between the densities of states of the Cr and Ag atoms, the presence of Ag atoms above and below

the buried Cr layer has a significant effect on the dispersion of the Cr states. However, the magnetic moments on the Cr atoms remain almost the same as they would be in a freestanding Cr monolayer that had been stretched to the Ag lattice constant.

Upon performing DFT+U calculations, we find that the best agreement between theory and experiment is obtained when U is set equal to zero, confirming that this is a system where electron correlation effects are relatively weak.

[1] V. Blum, Ch. Rath, S. Müller, L. Hammer, K. Heinz, J. M. García, J. E. Ortega, J. E. Prieto, O. S. Hernán, J. M. Gallego, A. L. Vázquez de Parga, and R. Miranda, Phys. Rev. B **59**, 15966 (1999).

[2] S. De Rossi, F. Ciccacci, and S. Crampin, Phys. Rev. B **52**, 3063 (1995).

[3] A. Kubetzka, M. Bode, O. Pietzsch, and R. Wiesendanger, Phys. Rev. Lett. **88**, 057201 (2002).

[4] P. Schieffer, C. Krembel, M. C. Hanf, G. Gewinner, and Y. Gauthier, Phys. Rev. B **65**, 235427 (2002).

[5] P. Schieffer, C. Krembel, M. C. Hanf, and G. Gewinner, Phys. Rev. B **57**, 1141 (1998).

[6] W. L. O'Brien and B. P. Tonner, Phys. Rev. B **51**, 617 (1995).

[7] B. Santos, J. M. Puerta, J. I. Cerda, R. Stumpf, K. von Bergmann, R. Wiesendanger, M. Bode, K. F. McCarty, and J. de la Figuera, New J. Phys. **10**, 013005 (2008).

[8] M. C. Hanf, C. Pirri, J. C. Peruchetti, D. Bolmont, and G. Gewinner, Phys. Rev. B **39**, 1546 (1989).

[9] A. Al-Zubi, G. Bihlmayer, and S. Blügel, Phys. Status Solidi B **248**, 2242 (2011).

[10] R. Moroni, F. Bisio, M. Canepa, and L. Mattera, Surf. Sci. **454-456**, 875 (2000).

[11] J. Dresselhaus, D. Spanke, F. U. Hillebrecht, E. Kisker, G. van der Laan, J. B. Goedkoop, and N. B. Brookes, Phys. Rev. B **56**, 5461 (1997).

[12] F. J. Himpsel, J. E. Ortega, G. J. Mankey, and R. F. Willis, Adv. Phys. **47**, 511 (1998).

[13] C. A. F. Vaz, J. A. C. Bland, and G. Lauhoff, Rep. Prog. Phys. **71**, 056501 (2008).

[14] M. A. Leroy, A. M. Bataille, Q. Wang, M. R. Fitzsimmons, F. Bertran, P. Le Fèvre, A. Taleb-Ibrahimi, A. Vlad, A. Coati, Y. Garreau, T. Hauet, C. Gatel, F. Ott, and S. Andrieu, Appl. Phys. Lett. **107**, 251602 (2015).

[15] A. J. Freeman and C. L. Fu, J. Appl. Phys. **61**, 3356 (1987).

[16] C. L. Fu and A. J. Freeman, Phys. Rev. B **33**, 1755 (1986).

[17] C. L. Fu, A. J. Freeman, and T. Oguchi, Phys. Rev. Lett. **54**, 2700 (1985).

[18] S. Blügel, M. Weinert, and P. H. Dederichs, Phys. Rev. Lett. **60**, 1077 (1988).

[19] S. Blügel, B. Drittler, R. Zeller, and P. H. Dederichs, Appl. Phys. A **49**, 547 (1989).

[20] S. Blügel, Phys. Rev. Lett. **68**, 851 (1992).

[21] E. Fawcett, Rev. Mod. Phys. **60**, 209 (1988).

[22] H. Zabel, J. Phys.: Condens. Matter **11**, 9303 (1999).

[23] J. Das, S. Biswas, A. K. Kundu, S. Narasimhan, and K. S. R. Menon, Phys. Rev. B **91**, 125435 (2015).

[24] C. Krembel, M. C. Hanf, P. Wetzel, C. Pirri, J. C. Peruchetti, D. Bolmont, and G. Gewinner, Vacuum **41**, 460 (1990).

[25] C. Krembel, M. C. Hanf, J. C. Peruchetti, D. Bolmont, and G. Gewinner, Phys. Rev. B **44**, 8407 (1991).

[26] C. Krembel, M. C. Hanf, J. C. Peruchetti, D. Bolmont, and G. Gewinner, J. Magn. Magn. Mater. **93**, 529 (1991).

[27] D. Rouyer, C. Krembel, M. C. Hanf, D. Bolmont, and G. Gewinner, Surf. Sci. **331-333**, 957 (1995).

[28] C. Krembel, M. C. Hanf, J. C. Peruchetti, D. Bolmont, and G. Gewinner, J. Magn. Magn. Mater. **119**, 115 (1993).

[29] D. Rouyer, C. Krembel, M. C. Hanf, D. Bolmont, and G. Gewinner, Surf. Sci. **287-288**, 935 (1993).

[30] M. C. Hanf, C. Krembel, and G. Gewinner, Surf. Sci. **519**, 1 (2002).

[31] M. C. Hanf, C. Krembel, D. Bolmont, and G. Gewinner, Phys. Rev. B **68**, 144419 (2003).

[32] C. Krembel, M. C. Hanf, J. C. Peruchetti, D. Bolmont, and G. Gewinner, Phys. Rev. B **44**, 11472 (1991).

[33] J. F. Lawler, R. G. P. van der Kraan, H. van Kempen, and A. J. Quinn, J. Magn. Magn. Mater. **165**, 195 (1997).

[34] A. J. Quinn, J. F. Lawler, R. Schad, and H. van Kempen, Surf. Sci. **385**, 395 (1997).

[35] J. Das, A. K. Kundu, and K. S. R. Menon, Vacuum **112**, 5 (2015).

[36] J. Das, K. S. R. Menon, and A. K. Kundu, Adv. Sci. Lett. **22**, 232 (2016).

[37] C. Krembel, M. C. Hanf, J. C. Peruchetti, D. Bolmont, and G. Gewinner, Surf. Sci. **269-270**, 748 (1992).

[38] G. Allan, Phy. Rev. B **44**, 13641 (1991).

[39] S. K. Mahatha and K. S. R. Menon, Curr. Sci. **98**, 759 (2010).

[40] See http://www.quantum-espresso.org for QUANTUM ESPRESSO package; P. Giannozzi *et al.*, J. Phys.: Condens. Matter **21**, 395502 (2009).

[41] D. Vanderbilt, Phys. Rev. B **41**, 7892 (1990).

[42] J. P. Perdew, K. Burke, and M. Ernzerhof, Phys. Rev. Lett. **77**, 3865 (1996).

[43] M. Cococcioni and S. de Gironcoli, Phys. Rev. B **71**, 035105 (2005).

[44] H. Monkhorst and J. Pack, Phys. Rev. B **13**, 5188 (1976).

[45] N. Marzari, D. Vanderbilt, A. De Vita, and M. C. Payne, Phys. Rev. Lett. **82**, 3296 (1999).

[46] G. Cipriani, D. Loffreda, A. Dal Corso, S. de Gironcoli, and S. Baroni, Surf. Sci. **501**, 182 (2002).

[47] T. G. Dargam, R. B. Capaz and B. Koiller, Phys. Rev. B **56**, 9625 (1997).

[48] T. B. Boykin and G. Klimeck, Phys. Rev. B **71**, 115215 (2005).

[49] W. Ku, T. Berlijn, and C.-C. Lee, Phys. Rev. Lett. **104**, 216401 (2010).

[50] V. Popescu and A. Zunger, Phys. Rev. B **85**, 085201 (2012).

[51] P. V. C. Medeiros, S. Stafström, and J. Björk, Phys. Rev. B **89**, 041407 (2014).

[52] M. M. Pant and S. K. Joshi, Phys. Rev. **184**, 639 (1969).

[53] J. R. Smith, F. J. Arlinghaus, and J. G. Gay, Phys. Rev. B **22**, 4757 (1980).

[54] E. C. Snow, Phys. Rev. **172**, 708 (1968).

[55] R. Courths, V. Bachelier, and S. Hüfner, Solid State Commun. **38**, 887 (1981).

[56] F. Venturini, J. Minár, J. Braun, H. Ebert, and N. B. Brookes, Phys. Rev. B **77**, 045126 (2008).

[57] E. D. Hansen, T. Miller, and T. C. Chiang, Phys. Rev. B **55**, 1871 (1997).

[58] P. Zhang, P. Richard, T. Qian, Y.-M. Xu, X. Dai, and H. Ding, Rev. Sci. Instrum. **82**, 043712 (2011).

[59] P. Steadman, C. Norris, C. L. Nicklin, N. Jones, and J. S. G. Taylor, Phys. Rev. B **64**, 245412 (2001).

[60] D. A. Luh, J. J. Paggel, T. Miller, and T.-C. Chiang, Phys. Rev. Lett. **84**, 3410 (2000).

[61] J. J. Paggel, D.-A. Luh, T. Miller, and T.-C. Chiang, Phys. Rev. Lett. **92**, 186803 (2004).

[62] C. Gray, Y. Lei, and G. Wang, J. Appl. Phys. **120**, 215101 (2016).

[63] B. N. Cox, M. A. Coulthardt, and P. Lloyd, J. Phys. F: Met. Phys. **4**, 807 (1974).